Measurement of mass attenuation coefficients in air by application of detector linearity tests

A. G. Peele, C. T. Chantler, D. Paterson, P. J. McMahon, T. H. K. Irving, J. J. A. Lin, and K. A. Nugent
School of Physics, University of Melbourne, Parkville, 3010, Australia

A. N. Brunton
X-Ray Astronomy Group, Department of Physics and Astronomy, University of Leicester, Leicester LE1 7RH, England

I. McNulty
Advanced Photon Source, Argonne National Laboratory, 9700 South Cass Avenue, Argonne, Illinois 60439

(Received 21 December 2001; revised manuscript received 30 July 2002; published 1 October 2002)

Accurate knowledge of x-ray mass attenuation coefficients is essential for studies as diverse as atomic physics, materials science, and radiation safety. However, a significant discrepancy exists between theoretical tabulated results for air at soft x-ray energies. We outline a precision measurement of the mass attenuation coefficients for air at various energies using two types of detectors and a simple test of detector response. We discuss whether sufficient accuracy can be obtained using this data to distinguish between competing theoretical estimates. In the process, we investigate the intensity response of two common synchrotron x-ray detectors: an x ray to optical charge-coupled device camera using a crystal scintillator and an x-ray sensitive photodiode.

DOI: 10.1103/PhysRevA.66.042702 PACS number(s): 32.80.Fb, 78.70.Dm

I. INTRODUCTION

It is important to know the properties of air for applications such as radiation safety (total attenuation) and x-ray fluorescence studies (relative attenuation). There have been recent comments that some tabulations of air attenuation are not accurate enough for these applications [1]. Furthermore, there has been little reported experimental data on the x-ray attenuation of this ubiquitous material. Some measurements were made around 1930 [2] and more measurements and compilations of measurements [3,4] were made around 1970, but since then, there has been a dearth of reported measurements.

This is the situation in spite of the fact that accurate measurement of mass attenuation coefficients can provide critical tests of theoretical calculations of the imaginary component of atomic form factors. The form factor is the resonant scattering amplitude of x rays by matter (primarily by electrons for x-ray energies). Form factors underlie major applications of x-ray crystallography, x-ray reflectometry, x-ray fluorescence, and x-ray anomalous fine structure. Consequently, particularly in the soft x-ray regime, it is important to understand the impact form factors will have on such experiments, and to verify the actual values of the form factors used.

The mass attenuation coefficient is related to the photoelectric cross-section σ by

$$[\mu/\rho]=\frac{\sigma}{uA}, \tag{1}$$

where u is the atomic mass unit and A is the relative atomic mass of the target element. For the elements in air and in our energy range ($1-2$ keV) the photoelectric cross-section σ_{PE} contributes $>99.9\%$ of the total attenuation of the beam. The photoelectric cross section is related to the imaginary component of the atomic form factor f'' by

$$f''(E)=\frac{E\sigma_{\mathrm{PE}}(E)}{2hcr_e}, \tag{2}$$

where h, c, and r_e are Planck's constant, the speed of light, and the classical radius of the electron, respectively, and E is the x-ray energy.

The real and imaginary parts of the atomic form-factor f are calculated using relativistic dispersion theory [5,6]. This calculation requires theoretic knowledge of the atomic wave functions for neutral, excited, and ionized atoms. Except for hydrogen, the atomic wave function for each element is not known precisely, leading to significant uncertainty in f. Chantler [7] gives a recent summary of approaches and improvements to the method of calculating f. Theoretical tabulations of f have been made by Chantler [8–10], while others including Scofield, Saloman, and Hubbell [11–18] (referred to, collectively, as Saloman *et al.*) have tabulated the related attenuation cross sections. Henke *et al.*, and Henke, Gullikson, and Davis [19–21] have provided a commonly used synthesis of experimental and theoretical results. Other theoretical tabulations such as those of Creagh and Hubbell [22], Cromer and Liberman [23,24], and Kissel, Pratt, and Roy, Kane, Kissel, and Pratt, and Pratt, Kissel, and Bergstrom Pratt [25–27] have been widely used in different communities.

The mass attenuation coefficient for air is calculated from the elemental coefficients by

$$[\mu/\rho]_{\mathrm{air}}=\sum_i W_i\left(\frac{\mu}{\rho}\right)_i, \tag{3}$$

where W_i is the fraction by weight of the components of air. We use for dry air $W_{\mathrm{nitrogen}}=0.755\,268$, $W_{\mathrm{oxygen}}=0.231\,781$, $W_{\mathrm{argon}}=0.012\,827$, and $W_{\mathrm{carbon}}=0.000\,124$ [28]. This composition is modified by humidity. The fraction by weight in moist air of water vapor is given by

$$\left(\frac{P_{\mathrm{sat}}}{R_w T}\right) \Big/ \rho_{\mathrm{moist}}, \tag{4}$$

where T is the temperature in degrees Kelvin, R_w is the gas constant for water vapor (461.5 $\mathrm{J\,kg^{-1}\,K^{-1}}$), and ρ_{moist} is given by Eq. (8) below. The saturation vapor pressure is given by

$$P_{\mathrm{sat}} = h \times 0.006\,11 \times 10^{7.5 T_C/(237.7+T_C)}, \tag{5}$$

where h is the relative humidity and T_C is the temperature in degrees Celsius.

Between 1–2 keV, for elements in air, Henke's values follow those of Saloman *et al.* to better than 1%. In this regime, the experimental weighting in Henke's tabulation is small so that Henke and Saloman *et al.* use essentially the same theoretical calculation. Away from absorption edges, the tabulations of Chantler and Saloman *et al.* are estimated by the authors to be accurate to 1%. However, the tabulations often differ by amounts that are significantly larger than 1%, as do experimental results. There are similar discrepancies with the other theoretic tabulations. In this work, we will consider only two of the more recent tabulations, those of Chantler and Saloman *et al.* For the elements in air at 1–2 keV, the discrepancy between the Chantler tabulation and Saloman *et al.* is about 5%. Accordingly, given a reasonable experimental accuracy, one should be able to discriminate between the tabulations.

We choose as our method of measuring the mass attenuation coefficients an approach that tests the linearity of a detector with incident intensity. The linearity of detector response with incident intensity is often assumed, especially in x-ray experiments where flux calibrations can be difficult. This can result in data obtained with different detectors being presented as a uniform data set with little or no examination of whether detector response affects the outcome. In some cases, detector response can be calibrated as part of an experiment, where a known spatial intensity distribution in the plane of the detector is measured [29]. Another known intensity distribution is that given by the attenuation of flux through an absorber as governed by the Beer-Lambert law

$$I = I_0 \exp(-\rho t[\mu/\rho]), \tag{6}$$

where I is the intensity at thickness t through the material, I_0 is the intensity at $t=0$, ρ is the density, and $[\mu/\rho]$ is the mass attenuation coefficient. Detector nonlinearity will lead to deviation from the Beer-Lambert law and specific causes of nonlinearity, such as an inadequate estimation of dark current and saturation, can be modeled and quantified from fitting of the attenuation data [30].

Atmospheric air has certain advantages in its choice as an absorber to investigate linearity via the Beer-Lambert law. It is freely available to every experimenter and has a $1/e$ attenuation length for soft x rays (1–2 keV) of the order of a centimeter. Also, the composition is well known, with the effect of pollutants being well below the 1% level in the mass attenuation coefficient [3].

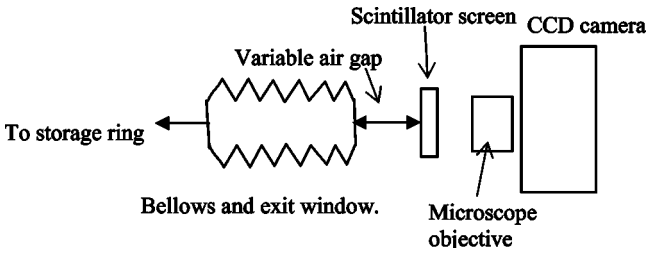

FIG. 1. Schematic of experimental setup for the CCD detector. For the ACP, the arrangement is similar.

II. EXPERIMENT

A. Setup

The experiments were performed at the 2-ID-B beamline at the Advanced Photon Source [31,32], Argonne National Laboratory. The flux available at the experimental station is $\sim 10^{12}$ ph/s/0.1% bandwidth. A monochromatic beam is obtained using a spherical grating monochromator. The monochromator was calibrated to the Si 1*s* edge inflection point in a total electron yield spectrum of a pure Si wafer. It is accurate to within an estimated 0.5 eV at 1839 eV. The calibration drifts at other energies due to a slight beam misalignment and is estimated to be accurate to within 2 eV at 1500 eV and 5 eV at 1200 eV [33]. We use these errors in our fitting as 1σ estimates.

We took measurements at each of these energies using an absolutely calibrated silicon photodiode (ACP) manufactured by International Radiation Detectors, Inc. [34]. This detector has *p* layer material at the active surface and *n* material forming the substrate. Together they form a *p*-*n* junction that operates as a photoelectric converter. When light strikes the photodiode, electron-hole pairs are formed in proportion to the amount of incident light and charge accumulates. The response of these detectors in terms of the collection mechanism and dark current effects is well understood [35].

Measurements were also taken at 1.5 keV using a cerium-doped yttrium aluminum garnet scintillator crystal, a microscope objective, and a low-noise charge-coupled device (CCD) camera manufactured by Princeton Instruments, Inc. (collectively referred to as the CCD detector). X-ray photoelectric absorption in the crystal gives rise to the emission of optical photons. The crystal, which is 500-μm thick and has a 5-μm deep layer doped with cerium, is transparent to visible light and the luminescence is focused by the microscope objective onto a standard CCD camera, which has high-detection efficiency in the visible range. Away from absorption edges, such scintillators are essentially calorimetric in nature and respond linearly to the incident intensity over several orders of magnitude. CCD detectors are also known for their excellent linearity. However, we are unaware of any work establishing the linearity of this specific detector response.

The detector was mounted close to the 700×700 $\mu\mathrm{m}^2$ exit window. The exit window is mounted on bellows and was scanned along the beam path in order to vary the air gap to the detector. A schematic of the experiment is shown in Fig. 1. The synchrotron storage ring was operating in its standard mode, which means that an initial ring current of

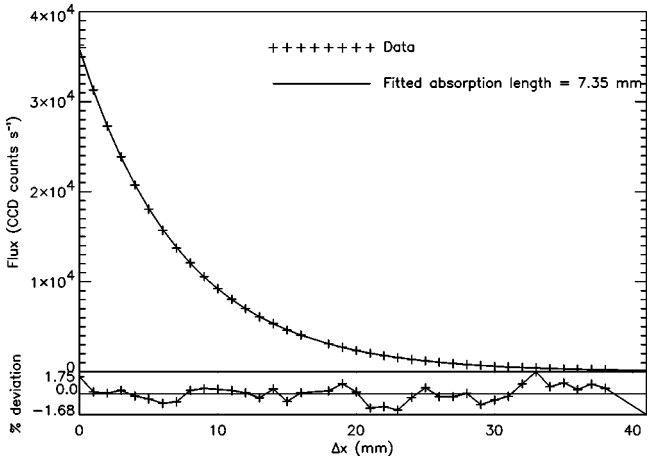

FIG. 2. Flux as a function of increasing air gap for the CCD detector for 1.5 keV incident energy. The attenuation law fit and deviations between the fit and the data are also shown. The experimental error bars are less than the linewidth at the lower end of the curve, while at the upper end, the vertical error bars are approximately equal in size to the plotting symbol.

approximately 100 mA was injected and allowed to decay until the next fill 12 h later.

B. Attenuation measurements

Figure 2 shows the measured CCD counts as a function of detector distance from the exit window measured at a monochromated beam energy of 1.5 keV. We fit the data to the simple Beer-Lambert form [Eq. (6)]. The fit is also shown in Fig. 2 with the lower panel showing the percentage deviation of the data from the fit.

In Fig. 3, we show one of two results for the ACP at a monochromated beam energy of 1.5 keV. The fit parameter from Eq. (6) is $\rho[\mu/\rho]$, which is the inverse of the attenuation length. The measured attenuation length from the CCD data

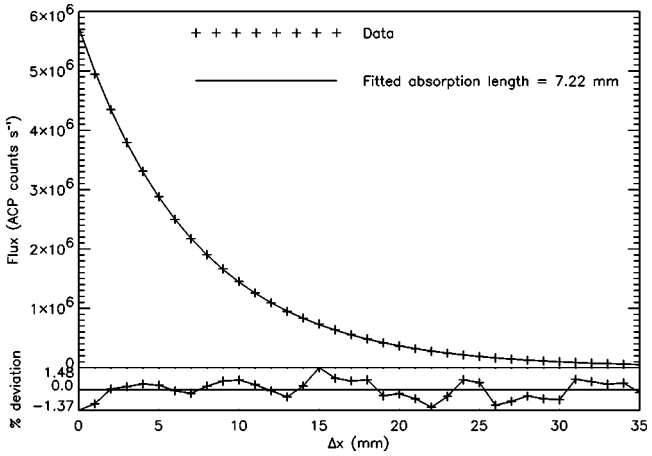

FIG. 3. Flux as a function of increasing air gap for the ACP detector for 1.5 keV incident energy. The attenuation law fit and deviations between the fit and the data are also shown. The experimental error bars are less than the linewidth at the lower end of the curve, while at the upper end, the vertical error bars are approximately equal in size to the plotting symbol.

is 7.35 mm with a three standard deviation uncertainty of 0.03 mm. The result averaged for the two ACP measurements is 7.25 ± 0.043 mm. The attenuation lengths obtained only differ by about 1%, thus demonstrating linearity in the detectors within the individual data point error (discussed below) of approximately 2%.

C. Fluctuations of signal

Typically, the ring current is monitored and used to normalize flux during an experiment. However, ring current monitoring can be insensitive to certain types of beam fluctuations, for instance, where the beam shifts relative to entrance slits, collimators, or monochromators [36,37]. We normalize against a fit to the decay of the ring current to account for the long-term decrease in the beam flux. Ideally, short-term fluctuations would be normalized out of final results by monitoring the flux with a detector upstream of the experiment. This can be difficult below 2 keV where attenuation through a detector may be significant. Accordingly, we estimate a combined flux and detector error for short-term fluctuations based on short-term monitoring of the beam with the experiment detector. Using the CCD detector, we obtained repeated exposures, taken continuously, of regions of the x-ray beam. For instance, one set of 12×10 exposures of 5 sec each imaged slightly different regions of the direct beam in each group of 10. Thus, we could calculate a standard deviation for each group of 10 and average across the 12 different sets. This process was repeated with different exposure times ranging between 1–10 sec and for different set sizes ranging from a single set of five exposures to 14 sets of 10 exposures. In all, 1254 standard deviations were calculated. The average standard deviation (weighted by number of sets) was 0.8% of the total flux in an exposure.

For the ACP, the combined beam and detector flux error was also estimated by monitoring the beam. Readings were taken at the same frequency as in corresponding attenuation measurements (1 sec) and the beam was monitored for a period five times longer than it took to obtain an attenuation measurement (typically 150 sec). The standard deviation for the ACP was 0.6%.

Cursory examination of the monitoring data shows that adjacent points are correlated. This can also be seen in the residuals to the fits in Figs. 2 and 3. This is tentatively assigned to a variation in the beam itself, as has been observed elsewhere [30]. This variation is not normally distributed, and creates larger probabilities of outliers than would be expected in a normal distribution. To take an account of this tail distribution and provide a robust experimental uncertainty, we report our experimental error estimate as three times the standard deviation ($\pm 3\sigma$), which results in an individual data point error for both detectors of $\sim 2\%$. This results in residuals that are consistent with this error estimate in our fits to the data as shown in Figs. 2 and 3. Quantifying the normally and non-normally distributed components could provide a better estimate of the experimental accuracy but is not warranted since the estimates of point-wise variation lie within the ($\pm 3\sigma$) fitting uncertainty.

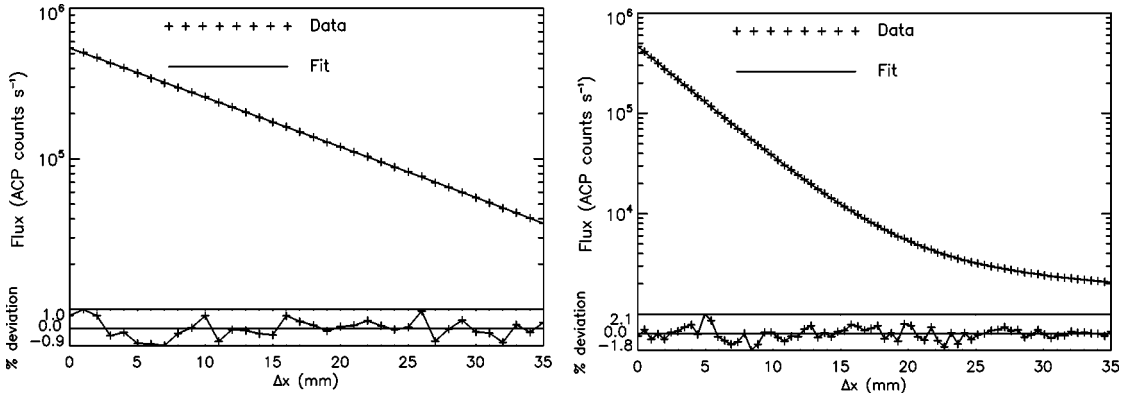

FIG. 4. Flux as a function of increasing air gap for the ACP detector for 1.83 keV (on the left) and 1.2 keV (on the right) incident energies. The plots are shown on a log-linear scale here so that the need for a harmonic component in the fit at 1.2 keV can be seen. At 1.83 keV (as is also the case at 1.5 keV) a straight line is observed validating the assumption of monochromaticity in the beam. At 1.2 keV, the effect of the 2.4-keV harmonic can be seen in the deviation from a straight line.

D. Offset correction

The final signal is obtained for the CCD by subtracting from each measurement an offset count defined by the counts recorded with the shutter open but the x-ray beam switched off. This ensures that ambient light in the experimental enclosure, as well as any dark current term in the detector, is subtracted. The error for the offset count was estimated in the same way as for the CCD signal error and has an upper estimate of 0.3% of the offset count. The value is smaller than that obtained for the signal as there are no beam fluctuations. The offset count was in all cases less than 3% of the signal flux. Accordingly, the net error in the data after subtraction of the offset count is not significantly increased. The ACP offset is adjusted electronically at the preamplifier so that ambient conditions with the x-ray beam off give a zero count rate. It has been shown that where attenuation measurements are extended far enough, typically beyond $I/I_0 < 0.0003$, it is possible to quantify the offset error from fitting to the attenuation curve [30]. Where this type of modeling is done, relative thickness measurements are no longer sufficient and absolute thickness measurements of the absorber are required.

III. MASS ATTENUATION COEFFICIENTS

The measurement shown in Fig. 2 was repeated and measurements at 1.83 and at 1.2 keV were obtained, as illustrated on a log-linear plot in Fig. 4. It is obvious that the 1.2-keV data set is affected by a significant higher-order harmonic component, as noted by the change in slope on the plot, compared to that for the other energies. At 1.2 keV, we found that the fit was significantly improved by including the effect of an energy harmonic as follows:

$$I = I_0[(1-\eta)\exp(-\rho t[\mu/\rho]_{1.2}) + \eta\exp(-\rho t[\mu/\rho]_{2.4})], \tag{7}$$

where $[\mu/\rho]_{1.2}$ and $[\mu/\rho]_{2.4}$ are the mass attenuation coefficients at 1.2 keV and at its second harmonic at 2.4 keV and where η is the fraction of harmonic contamination. We find harmonic contamination of 1%. Although the grating can be designed to reject such harmonics, gratings are usually optimized over a narrow energy range, and in general, the appearance of a harmonic occurs over a relatively narrow change of energy [30]. In our case, this is expected to happen below 2.8 keV due to the presence of a pair of rhodium coated mirrors operated at a grazing incidence angle of 1.25°. Taking into account the beam spectrum and the efficiency of the grating, the harmonic content is estimated to be well below the 1% level for fundamental energies above 1.4 keV. This is apparent from the fact that a two-energy model does not improve the fit for the measurements at 1.5 and 1.83 keV. However, if the attenuation measurements were extended, then we should be able to quantify the harmonic content down to well below the 1% level [30].

For the density of moist air we use the following equation recommended by the Comité International des Poids et Mesures [38]:

$$\rho = \frac{PM_a}{Z(P,T)RT}\left[1 - h\frac{f(P,T)P_{\mathrm{sat}}^2}{100R_wPT}\left(1-\frac{M_v}{M_a}\right)\right], \tag{8}$$

where P is the pressure (Pa), M_a is the molar mass of standard composition dry air corrected for the measured molar fraction of CO_2, (x_{CO_2}), $[28.9635 + 12.011(x_{CO_2} - 0.0004) \times 10^{-3}\ \mathrm{kg\,mol^{-1}}]$, R is the gas constant for dry air $(8.31451\ \mathrm{J\,mol^{-1}\,K^{-1}})$, R_w is the gas constant for water vapor $(25.6175\ \mathrm{J\,mol^{-1}\,K^{-1}})$, and M_v is the molar mass of water vapor $(18.015\ \mathrm{kg\,mol^{-1}})$. The compressibility factor Z and the enhancement factor f are both well-defined empirical functions of P and T [38].

The biggest source of uncertainty in our measurements was the calculation of the density due to uncertainty in the temperature (±1 °C) and pressure. The stability of both temperature and pressure was better than 0.1%, but our absolute estimates were relatively poor. Accordingly, we first perform a minimization of $\chi^2 = \Sigma(\mathrm{data} - \mathrm{tabulation})^2/\Sigma(\mathrm{tabulation})^2$ between the data and the tabulations as a function of pressure and temperature to determine if one tabulation gives a more

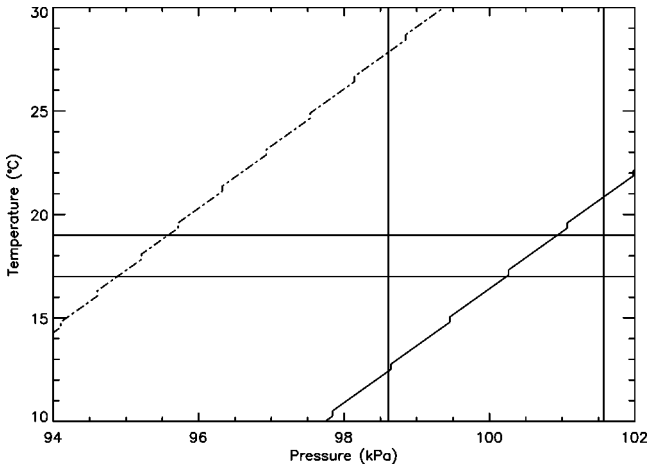

FIG. 5. The diagonal lines show the locus in pressure and temperature of the minimized χ^2. The dashed line at the left is for the tabulation of Saloman *et al.*, the solid line is for the tabulation of Chantler. The horizontal lines show the acceptable temperature range for the experiment. The vertical lines indicate the estimated experimental pressure range based on that recorded by the exterior weather station.

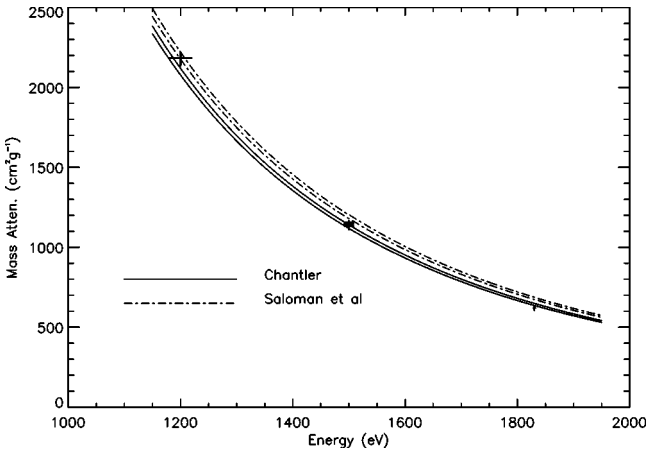

FIG. 6. The tabulated and experimental values for the mass attenuation coefficient as a function of energy. The tabulated curves are those of Chantler and of Saloman *et al.* as discussed in Sec. I. The tabulated curves show the 1% error bounds on the theoretic values for the experimental parameters.

consistent fit to the data, or, in the case where consistent fits can be found for both tabulations, whether the temperature and pressure parameters so determined are reasonable. The tabulations are calculated using the density and the composition of moist air by weight, which may be obtained from Eqs. (3)–(5) and (8) for $P=100.6$ kPa, $T=18\,^{\circ}$C, and relative humidity of 30% as 1.201 mg cm^{-3} and: $W_{\text{nitrogen}}=0.753\,474$, $W_{\text{oxygen}}=0.233\,340$, $W_{\text{argon}}=0.012\,797$, $W_{\text{carbon}}=0.000\,124$, and $W_{\text{hydrogen}}=0.000\,266$. The mass attenuation coefficient data is calculated using Eqs. (6) or (7) as appropriate. Accordingly, we measure the mass attenuation coefficients at 1.2, 1.5, and 1.83 keV as

$$[\mu/\rho]_{1.2}=2186^{+50}_{-35}\ \text{cm}^2\,\text{g}^{-1},$$

$$[u/\rho]_{1.5}=1153,1145,1133^{+23}_{-14}\ \text{cm}^2\,\text{g}^{-1};\ \text{and}$$

$$[\mu/\rho]_{1.83}=621^{+15}_{-11}\ \text{cm}^2\,\text{g}^{-1}.$$

We use asymmetric error bars based on our estimation of the likely pressure range, which propagates through as discussed below.

Figure 5 shows the locus in pressure and temperature of the minimized χ^2 for the tabulations of Chantler and Saloman *et al.* The horizontal lines show the range in the estimated temperature. The pressure measurement has some uncertainty, since we only have a contemporaneous accurate measurement from a nearby outdoor weather station of 98.61 kPa. Due to heating in the closed building and the experiment hutch, the experimental pressure is expected to be greater than this (but no less), by an amount (based on noncontemporaneous checks of the pressure) of perhaps up to 3 kPa.

Based on Fig. 5, we favor the tabulation of Chantler at a pressure of 100.6 kPa, which is within the estimated pressure range. Alternatively, we reject the tabulation of Saloman *et al.* as there is no temperature and pressure pair that minimizes χ^2 and which falls within the experimental temperature and pressure range.

Figure 6 shows the data at a density corresponding to a temperature of $18\pm1\,^{\circ}$C and pressure of $100.6+1.0-2.0$ kPa (using asymmetric error bars based on our estimation of the pressure range). Also shown are the tabulated values of Chantler and Saloman *et al.*, where the claimed 1% error range is shown as two curves for each tabulation. The agreement with Chantler is extremely good with only one energy (1.2 keV) perhaps favoring the Saloman *et al.* result, while the data at all three energies considered together clearly favors the Chantler tabulation as discussed in relation to Fig. 5.

IV. CAUSE OF DISCREPANCY

We have already discussed some of the experimental causes for discrepancy between theory and experimental results. Other sources of discrepancy are not expected to be applicable to this experiment. This includes near-edge solid state or molecular x-ray anomalous fine structure (XAFS) as there are no nearby edges for any of the major constituents of air, and of course because the medium is a gas. Soft x-ray resonances can occur, and would be reflected in a discrepancy of theory with experiment, but in our energy region resonances are only expected for high-Z elements. Molecular form factors differ from atomic ones, but only at lower energies than used in this experiment, so the atomic tabulations should be reasonable in this energy range for the constituent elements. The tabulated theories of Chantler and Saloman *et al.* both neglect XAFS, soft x-ray resonances, and molecular corrections. Accordingly, possible differences in the treatment of these effects are not the cause of the discrepancy between the theories.

Hence, the cause of the discrepancy between theories

must be due to the discrepancies in the atomic form-factor predictions for the constituent gases. Argon shows a 6, 9, and 9% discrepancy at the three energies, between Saloman *et al.* and Chantler. Atomic oxygen shows a 5, 6, and 5.5% discrepancy between the tabulations at 1.2, 1.5, and 1.83 keV, respectively. Atomic nitrogen also shows 5, 5, and 6% discrepancies for the three energies. All these discrepancies follow the form indicated on Fig. 6, and experimental data for 1.5 and 1.83 keV appear quite convincingly to favor the Chantler formalism.

Scofield [11], as reported in Saloman, Hubbel, and Scofield [13], uses an unrenormalized formalism. Initially, Scofield recommended the possible use of renormalization of his results for the relativistic wave function at the nucleus. This was later rejected by Saloman, Hubbel, and Scofield as being discrepant from the available experimental data. Chantler uses the Dirac-Hartree-Fock code, so he already includes this.

The partial effect of renormalization is to reduce the cross section for the relativistic amplitude at the nucleus compared to the nonrelativistic value. In the case of nitrogen, the correction factors given by Scofield [11] are 0.9756 for the K shell and 0.8595, 0.7644, and 0.7589 for the L subshells. Since between 1 and 2 keV the K shell contributes 95.1–95.0% of the total photoabsorption cross section, with 4.4–4.7% from the $2s$ subshell, Scofield predicted a relativistic reduction by 3.1% across this range. Similarly for oxygen, Scofield predicts a K shell 94.7–94.8% contribution to the cross section across this range, leading to a predicted reduction by 2.4%. Argon is similarly affected but dominated by the L shell and M shell cross sections with reductions of about 5% but with a smaller compositional percentage in air and a similar absolute cross section. So Scofield's renormalized values would yield a reduction of the Saloman *et al.* values by approximately 2.9% in closer agreement with experiment; yet not as close as Chantler. Partly, this suggests the value of a fully relativistic Dirac formalism, assuming that convergence is equally uniform.

V. CONCLUSION AND FURTHER WORK

We have performed measurements of the x-ray mass attenuation coefficient for air at the energies of 1.2, 1.5, and 1.83 keV. This was done by using a simple test of detector linearity. Based on a plausibility argument, we favor the theoretical attenuation coefficient tabulation of Chantler over those of Saloman *et al.* However, we identify several areas where this type of experiment may be improved so that a direct measurement can be used to discriminate more critically between Chantler, the renormalized version of Scofield, and other theories. These areas include: pressure, temperature, and relative humidity-which can all be measured to higher accuracy; offset errors-which can be modeled if attenuation measurements are extended beyond $I/I_0 < 0.0003$ [30]; harmonic contamination-which can be modeled precisely at all energies if extended attenuation measurements are made [30]; and energy calibrations-which can be improved using calibrated detectors. The careful investigation of some of these details will require a high-performance insertion device synchrotron beamline in order to obtain the necessary dynamic range and energy tunability.

Following this approach, we believe it will be possible to reduce experimental uncertainties in the measured mass attenuation coefficients to below 1%. If so, then it will be possible to discriminate between advanced theoretical values and, by taking measurements over a range of energies, it may be possible to identify the contribution of the individual elements present to the net mass attenuation coefficient for air.

ACKNOWLEDGMENTS

T.H.K.I. acknowledges receipt of an Australian Research Council post-graduate award. This work was supported by the Australian Synchrotron Research Program, which is funded by the Commonwealth of Australia under the Major National Research Facilities Program, by the Australian Research Council, and by the U.S. Department of Energy, Basic Energy Sciences, Office of Science under Contract No. W-31-109-Eng-38.

[1] H. M. Blair and W. M. Poteet, Proc. SPIE **4129**, 494 (2000).
[2] See, for a summary, A. H. Compton and S. K. Allison, *X-Rays in Theory and Experiment* (Van Nostrand, New York, 1935), p. 521.
[3] J. H. McCrary, L. H. Zeigler, and L. D. Looney, J. Appl. Phys. **40**, 2690 (1969).
[4] Wm. J. Veigele, J. Appl. Phys. **41**, 3178 (1970).
[5] D. T. Cromer and D. Lieberman, J. Chem. Phys. **53**, 1891 (1970).
[6] M. S. Jensen, Phys. Lett. A **74**, 41 (1979).
[7] C. T. Chantler, Radiat. Phys. Chem. **41**, 759 (1993).
[8] C. T. Chantler, J. Phys. Chem. Ref. Data **24**, 71 (1995).
[9] C. T. Chantler, J. Phys. Chem. Ref. Data **29**, 597 (2000).
[10] See, also, http://physics.nist.gov/PhysRefData/FFast/Text/cover.html, which incorporates these results.
[11] J. H. Scofield, Lawrence Livermore National Laboratory Report No. UCRL-51326, 1973 (unpublished).
[12] E. B. Saloman and J. H. Hubbell, NBSIR 86-3431, 1986 (unpublished).
[13] E. B. Saloman, J. H. Hubbell, and J. H. Scofield, At. Data Nucl. Data Tables **38**, 1 (1988).
[14] J. H. Hubbell, Prog. Retinal Res. **70**, 58 (1977).
[15] J. H. Hubbell, H. A. Gimm., and I. Overbo, J. Phys. Chem. Ref. Data **9**, 1023 (1980).
[16] J. H. Hubbell, Int. J. Appl. Radiat. Isot. **33**, 1269 (1982).
[17] J. H. Hubbell, W. J. Veigele, E. A. Briggs, R. T. Brown, D. T. Cromer, and R. J. Howerton, J. Phys. Chem. Ref. Data **4**, 471 (1975); **6**, 615(E) (1977).
[18] See also http://physics.nist.gov/PhysRefData/Xcom/Text/XCOM.html, which incorporates many of these results.
[19] B. L. Henke, P. Lee, T. J. Tanaka, R. L. Shimabukuro, and B. K. Fujikawa, At. Data Nucl. Data Tables **27**, 1 (1982).
[20] B. L. Henke, J. C. Davis, E. M. Gullikson, and R. C. C. Perera, LBL-26259, 1988 (unpublished).

[21] B. L. Henke, E. M. Gullikson, and J. C. Davis, At. Data Nucl. Data Tables **54**, 181 (1993).
[22] D. C. Creagh and J. H. Hubbell, in *International Table for Crystallography*, Vol. C, edited by A. J. C. Wilson (Kluwer Academic, Dordrecht, The Netherlands, 1992), pp. 189–206.
[23] D. T. Cromer and D. Liberman, J. Chem. Phys. **53**, 1891 (1970).
[24] D. T. Cromer and D. A. Liberman, Acta Crystallogr., Sect. A: Cryst. Phys., Diffr., Theor. Gen. Crystallogr. **A37**, 267 (1981).
[25] L. Kissel, R. H. Pratt, and S. C. Roy, Phys. Rev. A **22**, 1970 (1980).
[26] P. P. Kane, L. Kissel, and R. H. Pratt, S. C. Roy, Phys. Rep. **140**, 75 (1986).
[27] R. H. Pratt, L. Kissel, and P. M. Bergstrom, Jr, in *Resonant Anomalous X-ray Scattering, Theory and Applications*, edited by G. Materlik, C. J. Sparks, and K. Fischer (Elsevier, North-Holland, 1994), pp. 9–33.
[28] Ed. D. R. Lide, *Handbook of Chemistry and Physics* (CRC Press, Boca Raton, 2001).
[29] D. Paterson, B. E. Allman, P. J. McMahon, J. Lin, N. Moldovan, K. A. Nugent, I. McNulty, C. T. Chantler, C. C. Retsch, T. H. K. Irving, and D. C. Mancini, Opt. Commun. **195**, 79 (2001).
[30] C. Q. Chan, Z. Barnea, M. de Jonge, B. B. Dhal, D. Paterson, D. J. Cookson, and C. T. Chantler, X-Ray Spectrom. (to be published).
[31] I. McNulty, A. Khounsary, J. Barraza, C. Benson, Y. P. Feng, and D. Shu, Rev. Sci. Instrum. **67**, 3372 (1996).
[32] Z. H. Levine, S. Grantham, and I. McNulty, Phys. Rev. B **65**, 064111 (2002).
[33] I. McNulty (private communication).
[34] International Radiation Detectors Inc., 2527 West 237th Street Unit C, Torrance, CA 90505-5243, Model AXUV-100-Ti2.
[35] E. M. Gullikson, R. Korde, L. R. Canfield, and R. E. Vest, J. Electron. Spectrosc. Relat. Phenom. **80**, 313 (1996).
[36] C. T. Chantler, C. Q. Tran, D. Paterson, Z. Barnea, and D. J. Cookson, X-Ray Spectrom. **29**, 449 (2000).
[37] C. T. Chantler, C. Q. Tran, D. Paterson, Z. Barnea, and D. J. Cookson, X-Ray Spectrom. **29**, 459 (2000).
[38] R. S. Davis, Metrologia **29**, 67 (1992).